# Torque Estimation Technique for a Harmonic Drive Robotic Arm

Wen-Hao Chen, Ding-Chun Hsieh, Jyun-Yu Lin, and Chun-Yeon Lin, *Member, RST*

***Abstract*—This paper presents a double-axes torque estimation model for a harmonic drive actuator (HDA) robotic arm. Harmonic drives are known for their high gear ratio and relatively compact torque capacities. They have been widely implemented in robot manipulators, where accurate measurement or estimation of torque is necessary. However, the hysteresis property and related disturbances must be addressed when modeling. To model hysteresis, the wave generator and the flexspline were analyzed individually to fully consider their compliance. The structure of the system was carefully analyzed and designed to reduce deformation and exert torque from gravity. The angular displacement and torque can be measured and estimated, which enables the force estimation of the end effector. The model was numerically verified with constant and sinusoidal input, and the overall system, including the developed sensor, was verified through experiments.**

***Index Terms*—Harmonic drive, torque estimation, robotic arm**

## I. Introduction

Recently, there have been more and more occasions in which robots and people have had to work together, such as assisting humans in the working environment and in exoskeletons for rehabilitation therapy [1], [2]. People's safety has drawn a lot of attention. One way to ensure safety is to provide torque measurements on the robotic arm. When contact occurs, the difference between the external and the exerted torque is calculated and generated corresponding to compliant responses [3]. Information on intrinsic compliance with the joint is essential. In terms of stiffness regulation, flexible joints can be categorized into series of elastic actuators and variable stiffness actuators. The capability of the compliance to be regulated broadens the bandwidth limitation and facilitates adaptation to the environment for human–robot interaction [4].

A common method is implemented through direct torque sensing, which allows for a high sampling frequency and calculating precision. However, cost, system complexity, and reliability must be considered. Torque estimation methods, including harmonic drive instead of direct torque sensing, have been developed and serve as good alternatives. The harmonic drive has simple mechanisms, high gear ratios, and zero backlashes [5]. The torque sensing principle developed using harmonic drives is based on an internal component called the flexspline, which has relatively low torsional stiffness. Two approaches were introduced to measure the deformation of the flexspline, which was then mapped to the harmonic drive torque. The first approach utilized a strain gauge sensor. A joint torque sensor using a strain gauge was designed and optimized to achieve high sensitivity while maintaining high sensor stiffness [6]. The other used two high-precision angular encoders, which have already been integrated into many robotic and motion control architectures [7]. A method for estimating joint torque was introduced in which the position measurements of the motor-side and link-side encoders were substituted into a harmonic drive compliance model [8]. Emmei [9] proposed a joint torque control method for in-wheel motor-type electric vehicles with double encoders in which a load-side-encoder was used and encoder resolution was considered. Strain gauge sensors have better rejection of nonaxial moment crosstalk and torque ripple but higher signal drift, which is opposite to encoder-based sensors. In terms of resolution, strain gauge sensors are limited by the resolution of analog to digital conversion, while encoder sensors are determined by the encoder resolution [10].

As for the mapping process, an accurate model is crucial to precise modeling. Note that two noise sources must be addressed when the torque sensor is embedded in the joint. The first source is the extra-axial torque due to the weight of the manipulator and loads. Bearings could solve this problem, but they take up excessive mass. The second source is the sinusoidal disturbance of the harmonic drive, which is called torque ripple. The torque ripple phenomenon on the flexspline of harmonic drives (introduced due to an elliptical-shaped wave generator) hinders the extraction of the applied torque from the measured torque [11]. The local torque ripple only influences the measuring accuracy when sensing is conducted on the harmonic drive [12]. The four methods for the torque sensors are organized as follows: The first utilizes four strain gauges in the form of a Wheatstone bridge to minimize torque ripple. The second uses a Kalman filter [13]. The third involves a third sensor that cancels out the torque ripple by tuning the gain of each signal [14]. The last considers the joint speed and compensated torque ripple with an order-tracking technique [15]. In addition, friction at the joints and hysteresis behavior due to compliance and vibration must be considered.

Dhaouadi [16] proposed a new dynamic model by considering nonlinear stiffness and damping components and derived a nonlinear differential equation in which the parameters were obtained using optimization. Ruderman [17] proposed an extended model that builds upon the torsion-torque hysteresis map and nonlinear friction. With the concept of the virtual torsion sensor, the motor torques and velocity estimate and predict nonlinear joint torsion [17]. Zhang [18] proposed a method to model both the compliance and hysteresis properties by modeling the flexspline and the wave generator while considering the compliance of the wave generator to track hysteresis loss. As for noise and disturbance suppression in positioning, Iwasaki [5] proposed a compensator design to model the frequency characteristics of the vibration under the

This work was supported in part by National Taiwan University, under Grant NTU-CC-107L891001, NTU-CC-107L891001. (*Corresponding author: Chun-Yeon Lin*.)

The authors are with the Department of Mechanical Engineering, National Taiwan University, No. 1, Sec. 4, Roosevelt Road, Taipei, 10617, Taiwan. (r10522843@ntu.edu.tw; b08502053@ntu.edu.tw; r10522806@ntu.edu.tw; chunyeonlin@ntu.edu.tw)

assumption of a full-closed feedback positioning system. A disturbance observer is applied to make the dynamic characteristic from control input to deformation robust toward external noise [19]. Even though the disturbance observer provides decent robustness to the system, its performance impairs the noise problem. An integrated system consisting of a disturbance observer and a Kalman filter was proposed in [20], where the Kalman filter was used to reduce noise from measurement and estimation. This paper presents a modeling method for a two-axis Harmonic Drive Actuator (HDA) robotic arm and utilizes the rotary optical encoder to estimate the torque and angular displacement of the joints simultaneously. The remainder of this paper offers the following:

- The dynamics of the two-axis HDA robotic arm, which considers the compliance of the HDA, is modeled. A torque estimation technique and a joint-feedback control method based on the model are introduced, and the mechatronic system design of the two-axis HDA robotic arm is presented.

- The dynamics of the two-axis HDA robotic arm are numerically simulated. The torque estimation technique is numerically validated and implemented on the prototypes of a single-axis and two-axis HDA robotic arm.

## II. Torque Estimation Technique for a Harmonic Drive Robotic Arm

Fig. 1 illustrates the design concept of a two-axis flexible-joint robotic arm with HDA. As shown in Fig. 1(a), the robot arm joint used a direct current (DC) brushless motor with an HDA and was equipped with a developed torque-displacement sensor, which can be used to calculate the torque on the arm and the change in the angular position of the joint. In many applications, the force—or the reaction force—is applied to the robot end effector. Fig. 1(b) is the loading of HDA. $F_x$ and $F_y$ are the $x$ and $y$ components of the force exerted on the end effector, respectively. $F$ is the magnitude of the force. Fig. 1(c) is a schematic of the dynamics of the two-axis HDA robotic arm. The HDA is a flexible mechanism that includes a wave generator, a flexible wheel, and a gear ratio; the two brushless DC motors and the mechanical arm are rigid bodies. The two-axis HDA robotics arm model was composed of momentum of inertia, a spring, and a damper.

The torque of the motor side, the torque of the wave generator, the flexspline, the starting torque, and the external torque are $\tau_{m1,2}$ ,$\tau_{w1,2}$ ,$\tau_{f1,2}$ ,$\tau_{fs1,2}$ and $\tau_{d1,2}$ respectively. The angular displacement of the motor, the input side of the wave generator, the output side of the wave generator, the output side of the flexspline, and the arm are $\theta_{m1,2}$ , $\theta_{w1,2i}$, $\theta_{w1,2o}$, $\theta_{f1,2o}$, and $\theta_{1,2}$, respectively. The wave generator torsion is $\Delta\theta_{w1,2}$. The viscous friction $r_m$. $N$ is the gear ratio. $K_f$ is the stiffness of the flexspline.

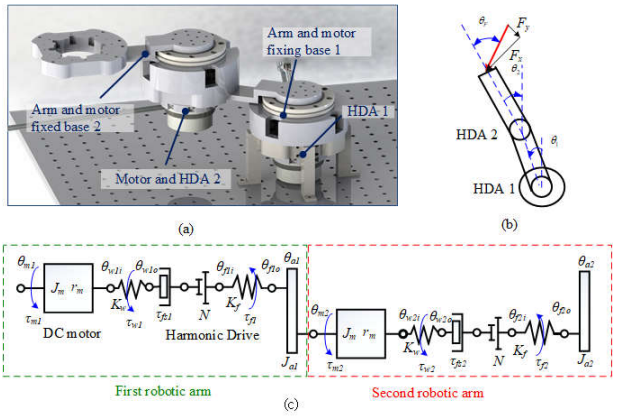


Fig. 1. Illustration of torque estimation technique for the two-axis HDA robotics arm. (a) Two-axis HDA robotic arm. (b) Loading of HDA. (c) Schematic illustration of the dynamics of the system.

### A. Model of the two-axis HDA robotic arm

The dynamic model of the two-axis HDA robotic arm is described in (1)–(5). $J_m$ and $J_a$ are the motor's inertia and the link sides' inertia, respectively. Since the motors used in the two axes were of the exact specification as the manipulator, the representation is the same. Thus, the wave generator output angle combines the motor angle and the wave generator torsion. The wave generator torsion is the difference between the output and input of the wave generator in (2). The relation between the wave generator torque and torsion is presented in (A.1). The torque of the flexspline was transmitted to the arm, and the external torque was also considered. The dynamic model of the DC motor is presented in (1). The viscous friction $r_m$, which can be obtained by (B.2) from the manufacturer. The flexspline torque is formulated in (3).

$$\tau_{m1,2} = J_m\ddot{\theta}_{w1,2o} + r_m\dot{\theta}_{w1,2o} + \tau_{w1,2} - \tau_{fs1,2} \tag{1}$$

$$\Delta\theta_{w1,2} = \theta_{w1,2o} - \theta_{w1,2i} \tag{2}$$

$$\tau_{f1,2} = K_f(\theta_{f1,2o} + \frac{\theta_{w1,2o}}{N}) \tag{3}$$

The dynamic models of the first and second arms are presented in (4) and (5), respectively. $N$ is the gear ratio. $K_f$ is the stiffness of the flexspline.

$$J_a\ddot{\theta}_1 = J_{a1}\ddot{\theta}_{f1o} = \tau_{f1} + \tau_{d1} \tag{4}$$

$$J_a\ddot{\theta}_2 = \tau_{f1} + \tau_{d1} + \tau_{f2} + \tau_{d2} \tag{5}$$

Fig. 2 shows the block diagram of this two-axis HDA robotic arm system.

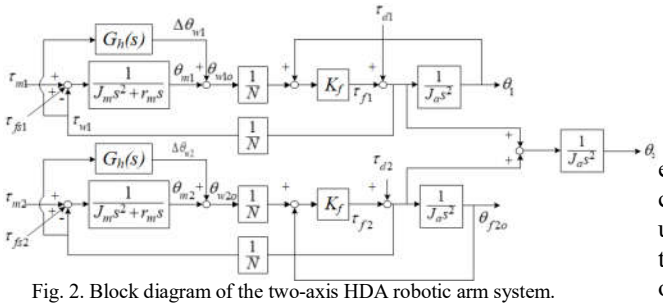

Fig. 2. Block diagram of the two-axis HDA robotic arm system.

### *B. Torque Estimation Method for the Two-joint HDA Arm*

The torque estimation method is based on the angular displacement measurement. The torsion angles of the wave generator are described by (2). The flexspline torsion of the first and second joint $\Delta\theta_{fk}$, $k \in 1,2$ are determined by

$$\Delta\theta_{fk} = \theta_{fok} - \theta_{fik}. \tag{6}$$

However, $\theta_{\omega ok}$, $\theta_{fik}$, $(k \in 1,2)$ are included in the structure of the harmonic drive, and both of the angular displacements cannot be measured directly. In Fig. 1(c), the relation of the $\theta_{\omega ok}$ and $\theta_{fik}$, $k \in 1,2$ can be determined by using the effect of the gear ratio as

$$\theta_{wok} = -N\theta_{fik}. \tag{7}$$

The total torsion $\Delta\theta$, $k \in 1,2$ is the difference between the input angular displacement of the wave generator and the output angular displacement of the flexspline, which can be described by

$$\Delta\theta_k = \theta_{fok} + \frac{\theta_{wik}}{N} \tag{8}$$

By substituting (2), (6), and (7) into (8), the torsion of the harmonic drive$\Delta\theta_{hk}$, $k \in 1,2$ is expressed as

$$\Delta\theta_h = \Delta\theta_f - \frac{\Delta\theta_w}{N} \tag{9}$$

The total torsion changes periodically, without any external torque, while the motor rotates. Thus, the kinematic torsion $\Delta\theta_t$ needs to be considered. The kinematic torsion is approximated by a five-order polynomial of $\theta$ as

$$\Delta\theta_t = \sum_{k=0}^{5} a_k \theta^k \tag{10}$$

The torsion angle only influenced by the external torque is to subtract the kinematic torsion from the torsion angle of the $k^{th}$ harmonic drive ( $k \in 1,2$ ), which can be determined by

$$\Delta\theta_k = \Delta\theta_{hk} + \Delta\theta_k \tag{11}$$

With (9) and (11), the flexspline torsion of $k^{th}$ joint ( $k \in 1,2$ ) can be obtained by

$$\Delta\theta_{fk} = \Delta\theta_k - \Delta\theta_{tk} + \frac{\Delta\theta_{wk}}{N}. \tag{12}$$

Finally, the estimated torque can be obtained by substituting (12) into (B.2) as

$$\tau_{est} = \frac{\tan((\Delta\theta_k - \Delta\theta_t + \frac{\Delta\theta_{wk}}{N})c_f K_{f0})}{c_f} \tag{13}$$

The two-axis HDA robotic arm had two rotary optical encoders to estimate the two-axis torque and to inversely calculate the external force of the link sides on the plane. An unknown external force was applied to the end of the arm, and the respective angular displacements of the two axes were obtained through the rotary optical encoder. The magnitude of external torque and the angle between the external torque and the second axis can be inverse computation. The length of a single arm is $l_a$. $F_x$ and $F_y$ in (14a, b) represent the $x$ and $y$ components of the force exerted on the end effector, respectively. $F$ is the magnitude of the force in (14c).

$$F_x = \frac{\tau_{\theta_2}}{\ell_a} = \frac{\tan((\Delta\theta_{f2} c_f K_{f0})}{c_f \ell_a} \tag{14a}$$

$$F_y = \frac{\tan(\Delta\theta_{f2} c_f K_{f0})(1+\ell_a \cos\theta_2) - \tan((\Delta\theta_{f1} c_f K_{f0})}{c_f \ell_a} \tag{14b}$$

$$F = \sqrt{F_x^2 + F_y^2} \tag{14c}$$

As shown in Fig. 1(c), by substituting the angular displacement $\Delta\theta_{fk}$ in (6) into (14a-c), the angle between the external force and the second axis ($\theta_f$) can be obtained by

$$\theta_F = \arctan\left(\frac{\tan(\Delta\theta_{f2} c_f K_{f0})\sin\theta_2}{\tan(\Delta\theta_{f2} c_f K_{f0})(1+\ell_a \cos\theta_2) - \tan((\Delta\theta_{f1} c_f K_{f0})}\right). \tag{15}$$

### *C. Joint Torque Feedback Control*

Fig. 3 illustrates the position control of the HDA system implemented with joint torque feedback to improve performance. The command position of the motor $\theta_r$ was controlled by the proportional-derivative (PD) controller in (16), where $K_P$ is the position feedback coefficient and $K_D$ is the velocity feedback coefficient. Both coefficients influenced the accuracy and stability of the HDA robotic arm system.

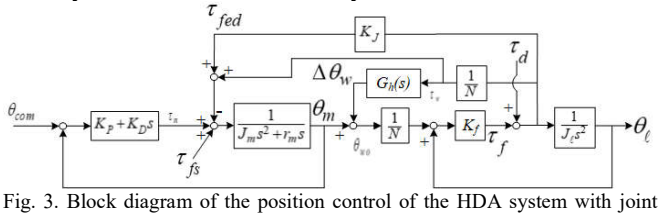

Fig. 3. Block diagram of the position control of the HDA system with joint torque feedback.

$$\tau_m = K_P(\theta_{com} - \theta_m) + K_D(\dot{\theta}_{com} - \dot{\theta}_m) \tag{16}$$

The feedback torque is expressed in (17), where $K_j$ is the joint torque feedback coefficient. The joint torque feedback coefficient was adjusted to change the performance of the HDA system. If the joint torque feedback coefficient was larger, the performance was more sensitive to external torque. Thus, the HDA system can reject the external torque or follow the external torque to achieve different tasks.

$$\tau_f = K_J(\tau_f + \tau_d) \tag{17}$$

### *D. Mechanical Design*

The two-axis HDA robotic arm was modularized. The

mechanism could be disassembled into three parts, as shown in Fig. 4: the base fixed to the optical table, the first set, and the second set of arms on the fixed base. The arm was driven by a motor and a HDA, and the torsion angle was measured using a rotary optical encoder. A set of arms was connected to the other set of arms by crossed roller bearings.

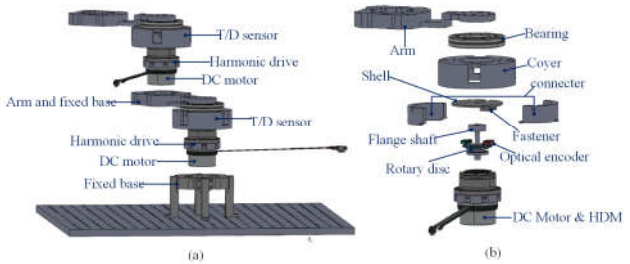


Fig. 4. Mechanical design. (a) Two-joint HDA robotic arm. (b) A set of arms with T/D sensor.

## III. Numerical Validation

The proposed torque estimation method for double-axis joints was verified with numerical simulations with the following two focuses. Time-domain and frequency response analyses of the two-axis HDA robotic arm were conducted, and the torque estimation technique was numerically validated.

### *A. Time Domain and Frequency Response Analysis of the Dynamic Model*

The verification process was conducted using MATLAB and Simulink in MATLAB. MATLAB Simscape Multibody was used to simulate the motion of the mechanism. The dynamic model to be verified was built to model the position output of both joints of the HDA robotic arm, which was designed in Solidworks and imported into MATLAB Simscape. The parameters of the HDA robotic arm are listed in Table I. The step and sinusoidal input currents were applied to the model. The simulated results of the output positions of the model are shown in Fig. 5. As shown in Fig. 5(a), The unit step input current will cause a continuous angular displacement that increases the positions of joints.In Fig. 5(b), the sinusoid input current increases the positions of joints with fluctuation.

TABLE I
PARAMETERS OF THE DOUBLE JOINT HDA ROBOTIC ARM

| | | | |
|---|---|---|---|
| $J_m$ | $1.21 \times 10^{-4}$ kgm$^2$ | $\tau_{fs}$ | 0.037 Nm |
| $J_\omega$ | $0.079 \times 10^{-4}$ kgm$^2$ | N | 100 |
| $J_\prime$ | 0.876 kgm$^2$ | $c_\omega$ | 27.027 (Nm)$^{-1}$ |
| $K_{\omega 0}$ | 2.5517 Nm/rad | $K_f$ | 10000 Nm/rad |
| $K_{f0}$ | 9743.939 Nm/rad | $c_f$ | 0.0831 (Nm)$^{-1}$ |
| $l_a$ | 0.15 m | | |

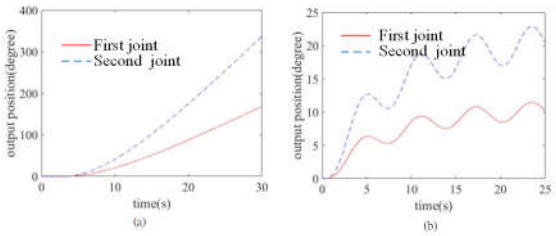


Fig. 5. Responses of position output of both joints. (a) Step input. (b) Sine input.

### *B. Numerical verification of the torque estimation*

Fig. 6 shows the simulation results of the link-side torque estimation for the first and second robotic arms. The parameters of the HDA robotic arm are listed in Table I. The real step input and estimated torque for the robotic arms are shown in Fig. 6(a)–(d). The close agreement between the estimated and measured torque validates the torque estimation method.

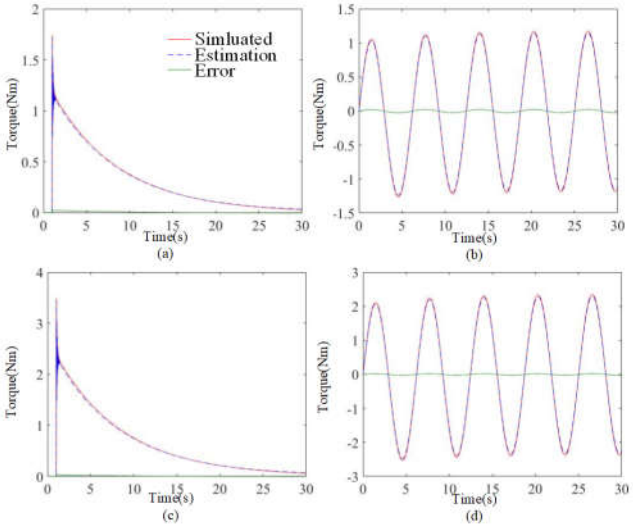


Fig. 6. Torque estimation with different inputs. (a) Estimated torque for the first robotic arm with step input and (b) sine input. (c) Estimated torque for the second robotic arm with step input and (d) sine input.

### *C. JOINT TORQUE FEEDBACK CONTROL*

The two simulations indicated the difference between with and without the joint torque feedback (JTF) of a single joint HDA. The first simulation was torque control, with $K_J = 1$. The second was position control with a PD controller with $K_J = 0.1$, $K_P = 0.003$, $K_D = 0.01$.

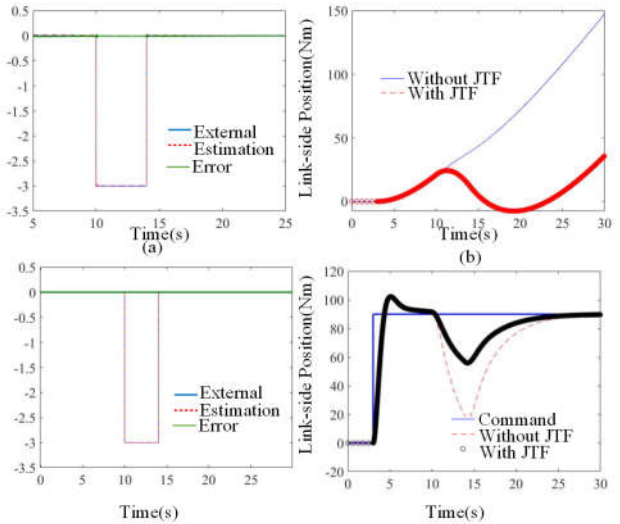


Fig. 7. The response of JTF in torque control mode. (a) Step external torque in the first simulation. (b) Comparison of the link-side position with and without JTF in the first simulation. (c) Step external torque in the second simulation. (d) Comparison of the link-side position with and without JTF in the second simulation.

To improve the torque compliance of the HDA system, the JTF coefficient was selected as -1. A step current was used as the input signal, and an external torque was applied between 10 and 15 seconds. The external torque and estimated torque are shown in Fig. 7(a). The link-side angular displacements with and without JTF are shown in Fig. 7(b). Without JTF, the motor followed the command input. Thus, the motor rotated in the same direction while external torque was applied. With JTF, the motor followed the direction in which the external torque is applied. The second simulation was based on position control. In the second simulation, the external torque applied as the same external torque in the first simulation is shown in Fig. 7(c). The result is shown in Fig. 7(d); the red dashed line is the displacement without JTF, and the blue line is the displacement with JTF. The results show that the influence of external torque can be compensated for with JTF. The link-side displacement with JTF was much smaller than the displacement without JTF due to external torque.

## IV. Experimental Results

Two experimental setups were conducted to validate the prototypes of the HDA robotic arms. The first was a single HDA joint to estimate static torque and constant torque input. The second was a two-axis robotic arm that moved in a horizontal plane to estimate static torque and constant torque input.

### *A. Verification of the static torque estimation of a single HDA joint*

Three experiments were conducted to validate the torque estimation accuracy for different situations. In the first experiment, external torque was applied to the arm while the DC motor was regulated in the same position. In the second experiment, external torque was applied while the DC motor rotated. The third experiment involved the application of joint torque feedback control. The experimental setup is shown in Fig. 8(a). External torque was applied to the link, which is the arm illustrated in the figure. The developed sensor was used to detect the angular displacement of the HDA for real-time torque estimation. It consisted of an optical encoder and an optical disc, as shown in Fig. 8(b). The six-axis force sensor measured the actual torque of the experiment and was responsible for validating the estimated torque. The National Instrument cRIO 9066 in Fig. 8(c) was used as the interface for input signal generation and data acquisition.

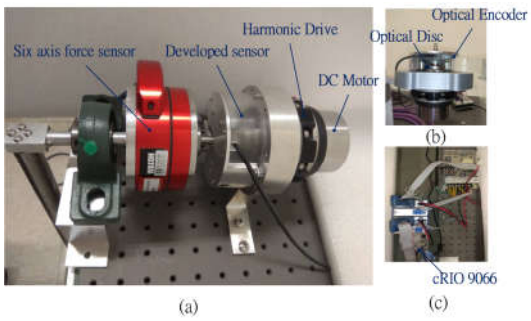


Fig. 8. Experimental setup. (a) HDA robotic arm. (b) Optical sensor for estimating angular displacement and torque. (c) Controller.

*Torque estimation for constant angular displacement and torque*

Fig. 9(a), (b) shows the experimental results of step external torque and periodic external torque. The estimated torques were calculated using (13). The torque was measured using a six-axis force-torque sensor. The differences between the estimations and measurements were due to the backlash between the flange shaft and the output load.

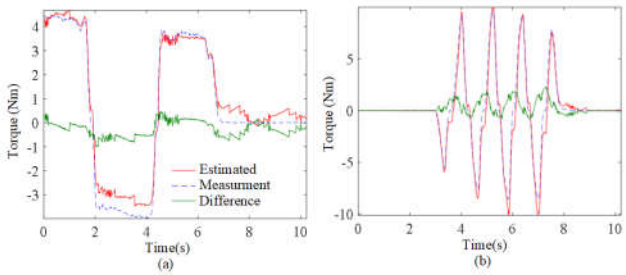


Fig. 9. Experimental results for constant angular displacement. (a) Periodic torque input. (b) Step torque input.

Another situation is the torque applied by the DC motor. A constant torque was applied to the DC motor to rotate a revolution. The torque was estimated while the motor rotated. First, kinematic torsion had to be eliminated to estimate torque. A 5th order polynomial in (10) approximates the kinematic torsion on the experimental data by the curve fitting method. The coefficients of kinematic torsion are listed in Table II. Fig. 10 demonstrates the kinematic torsion and the fitting curve. The kinematic torsion of the different input torques and directions is shown in Fig. 10(a). The results indicate that kinematic torsion is unique and associated only with angular displacement.

TABLE II
COEFFICIENTS OF THE KINEMATIC TORSION CURVE

| | | | | | |
|---|---|---|---|---|---|
| $a_0$ | $6.5719 \times 10^{-5}$ | $a_1$ | 0.0018 | $a_2$ | 0.0032 |
| $a_3$ | -0.0017 | $a_4$ | $2.6840 \times 10^{-4}$ | $a_5$ | $-1.2686 \times 10^{-5}$ |

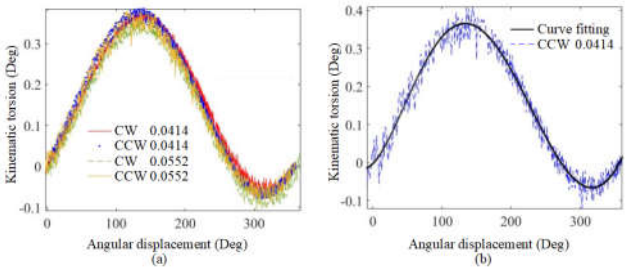


Fig. 10. The kinematic torsion for different inputs. (a) Estimation and measurement. (b) Curve fitting. (CW: clockwise; CCW: counterclockwise)

Fig. 11 shows the experimental results of the step external torque and periodic external torque. The measured and estimated torques are compared in Fig. 11(a) and 11(c), whose mean and maximum absolute differences were (1.27, 5.89) Nm and (1.33, 4.5), respectively. The leading cause of the difference may be the optical encoder, which is affected by the structure's vibration or some data acquisition issues. Fig. 11(b) and 11(d) show the corresponding angular displacement. The deviation from the supposed inclined line is because external torque was applied, which can be observed in the corresponding figure of the estimated torque.

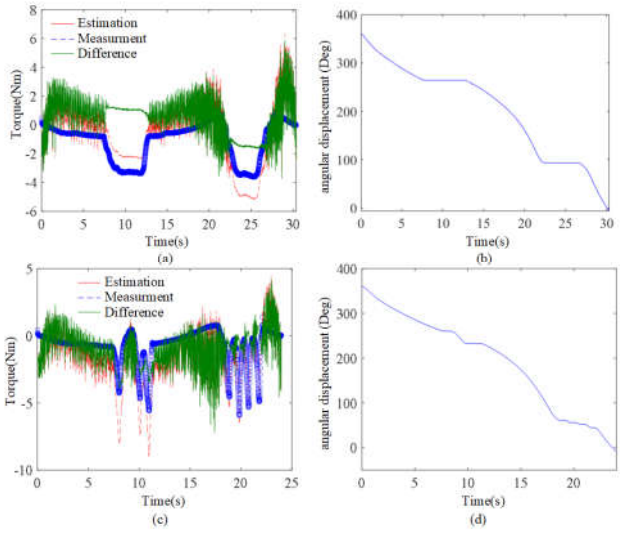


Fig. 11. Experimental results for constant torque. (a) (b) Step external torque; (c) (d) Periodic extremal torque (a, c: torque estimation; b, d: angular displacement).

*Joint torque feedback control*

In the first experiment, the DC motor generated constant torque, and the arm applied external torque as a disturbance. The link-side estimated torque and link-side position without JTF are shown in Fig. 12(a). The link-side estimated torque and link-side position with JTF are shown in Fig. 12(b). However, with the JTF, the motor rotated to follow the direction in which the external torque was applied. The results show that the JTF can give the HDA arm the ability to follow the external torque instead of resisting it.

In the second experiment, the command angular displacement was 90˚ and an external torque was applied to the arm. Fig. 12(c) shows the torque applied to the arm manually. Fig. 12(d) shows the results of the second experiment with and without the JTF. The results show that the angular displacement without JTF was larger than with JTF. In other words, rejecting external torque was higher in the HDA arm with JTF than without JTF.

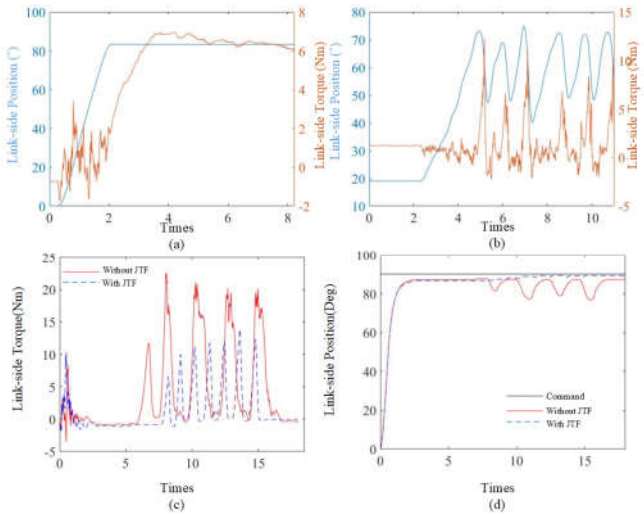


Fig. 12. Experimental setup and results of JFT control in two simulations. (a, b) First experiment (a: without JTF, b: with JTF). (c, d) Second experiment (c: estimated torque, d: angular displacement).

*B. Verification of static torque estimation of two-axis joints.*

The experiment setup of the two-axis HDA robotic arm, as shown in Fig. 13, consisted of a motor, HDA, optical scale, crossed roller bearing, and other mechanical components. The motor was a MAXON EC 60 flat, which can read the angular displacement of the motor side, and was controlled by the controller EPOS4 Compact 50/15 CAN with LabView program code; the harmonic drive was CSG-17-100-2UH-LW. Fig. 4(b) shows the exploded view of a set of the arm with T/D sensor. The optical scale is an indispensable element for torque estimation of the robot arm. The optical scale was an ARCDM-9405-4050RCDM 50 mm turntable with an ATOM4T1300 read head, which had high precision, a stable signal, and high resistance to good pollution ability. The read value was also read back to LabView for processing. One set of arms can add a degree of freedom to the system, and more complex goals can be achieved by adding multiple sets of arms. The planar motion structure allows free movement of both joints and gravitational force to be neglected in the model. Each joint comprises a motor, an HDA, and a developed sensor; the details are elaborated in Section IV.A.

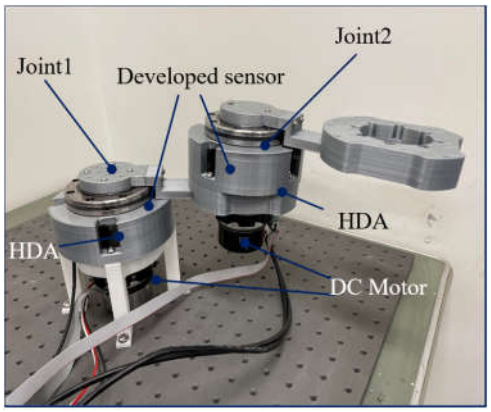


Fig. 13. Two-axis HDA robotic arm experiment setup.

Two scenarios were considered in the experiments. In the first scenario, the motors were not subjected to any input but external torque exerted on the arm. A random magnitude external torque was applied in the experiment. Fig. 14(a) shows the angular displacement and the estimated torque with random inputs without input currents to the motor. Torque and angular displacement had a positive relation. The noise peak had a property such that positive displacement would only have positive peaks, and vice versa, and those peaks mainly happened at places where the curve was relatively flat. The may be attributed to the sensor's resolution of the optical encoder. As the displacement curve went flat, the angle difference may have been too small for the high-resolution encoders to interpolate. The same phenomenon also occurred in the torque estimated from angular displacement. Due to the design of the double-joint mechanism, there is no spare space to install a 6-DOF sensor for further verification.

In the second scenario, the motor of Joint 1 was free from any input, while Joint 2 was applied with a constant torque of approximately 2.66 x$10^{-2}$Nm. The external torque was exerted by humans on the end-effector of the link. Kinematic torsion also affected the acquired data. To tackle kinematic torsion, some support was manually applied to the system, and the exerted

torque was applied conditionally so that no rapid angular displacement occurred at Joint 2. Fig. 14(b) shows the angular displacement and estimated overall torques with the input torque of 2.66 x10$^{-2}$Nm when the external torque is applied at 20~40, 40~60, 80~100 seconds by hand. A positive relation between torque and angular displacement can be observed.

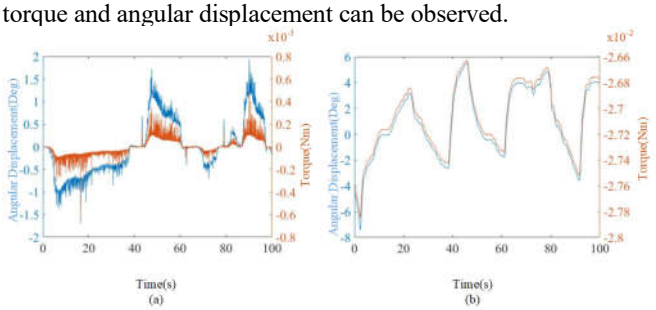


Fig. 14. Angular displacement and estimated torque with random external torques. (a) Without input currents to the motor. (b) With input currents to the motor.

## V. Conclusion

A torque estimation technique for a double-joint robotic arm considering modeling the hysteresis characteristic of the HDA has been presented. The hysteresis characteristic was modeled by taking the compliance property of the flexspline into account. A sensor using a rotary optical encoder to estimate torque and angular displacement was developed simultaneously. Step input and sinusoidal input were applied to both single-axis and two-axis robotic arm systems. The estimated torque was numerically verified by simulation.

Experiments were conducted under conditions that resembled the simulation. The actual harmonic drive and wave generator were investigated to verify the compliance model. The single-axis torque estimation results agreed with the measured torque. An application of the torque estimation technique to joint feedback control was illustrated. The torques of the two axes were estimated for the two-axis robotic arm. In the future, a six-axis force sensor will be equipped on the two joints to verify the torques. Joint torque feedback will be applied on the two-axis HDA robotic arm.

## Appendix A
## Motor Viscous Friction

The viscous friction of the motor $r_m$ is given in A.1, where $k_m$, $I_0$, and $n_0$ denote torque constant, no load current, and no load speed, respectively [21].

$$r_m = \frac{30 k_m I_0}{n_0 \pi} \tag{A.1}$$

## Appendix B
## Harmonic Drive Compliance Model

In the wave generator compliance model [18], the wave generator's torsional angle is given in (B.1), where $\psi$ is the hysteresis loss.

$$\Delta\theta_w = \frac{\mathrm{sgn}(\tau_w)}{c_w K_{w0}}(1 - e^{-c_w|\tau_w|}) \tag{B.1}$$

$$\text{where } c_w = \frac{2}{N K_{w0} \psi},\ K_{w0} = \frac{2T_{fs}}{N\psi}$$

The torque estimation method described by [18] is given in B.2, where $C_f$ and $K_{f0}$ can be determined from the parameters provided by the DC motor manufacturer.

$$\tau_{est0} = \frac{\tan(\Delta\theta_f C_f K_{f0})}{C_f} \tag{B.2}$$

## References

[1] C. Caulcrick, W. Huo, W. Hoult, and R. Vaidyanathan, "Human joint torque modelling with MMG and EMG during lower limb human-exoskeleton interaction," *IEEE Trans. Robot. Autom*., vol. 6, no. 4, pp. 7185-7192, Oct. 2021.
[2] W. Li, Y. Han, J. Wu, and Z. Xiong, "Collision detection of robots based on a force/torque sensor at the bedplate," *IEEE/ASME Trans. Mechatronics*, vol. 25, no. 5, pp. 2565-2573, Oct. 2020.
[3] D. Tsetserukou, R. Tadakuma, H. Kajimoto, N. Kawakami, and S. Tachi, "Intelligent variable joint impedance control and development of a new whole-sensitive anthropomorphic robot arm," in *Proc. CIRA, Jacksonville,* FL, USA, 2007, pp. 338-343.
[4] Y. Ning, Y. Liu, F. Xi, K. Huang, and B. Li, "Human-robot interaction control for robot driven by variable stiffness actuator with force self-sensing," *IEEE Access*, vol. 9, pp. 6696-6705, 2021.
[5] M. Iwasaki, "Robust full-closed control-based vibration suppression for positioning devices with strain wave gearing," in *Proc. of 12th France-Japan and 10th Europe-Asia Congr. on Mechatronics*, Tsu, Japan, 2018, pp. 11-17.
[6] B. Fu and G. Cai, "Design and calibration of a joint torque sensor for robot compliance control," *IEEE Sensors J.*, vol. 21, no. 19, pp. 21378-21389, Oct. 1, 2021.
[7] M. A. A. Ismail, J. Windelberg, and G. Liu, "Simplified sensorless torque estimation method for harmonic drive based electro-mechanical actuator," *IEEE Trans. Robot. Autom*., vol. 6, no. 2, pp. 835-840, Apr. 2021.
[8] H. Zhang, S. Ahmad and G. Liu, "Torque estimation for robotic joint with harmonic drive transmission based on position measurements," *IEEE Trans. Robot.*, vol. 31, no. 2, pp. 322-330, Apr. 2015.
[9] T. Emmei, S. Wakui, and H. Fujimoto, "Acceleration noise suppression for geared in-wheel-motor vehicles using double encoder," *IEEE Journal of Emerging and Selected Topics in Industrial Electronics*, vol. 2, no. 1, pp. 53-60, Jan. 2021.
[10] N. Kashiri, J. Malzahn, and N. G. Tsagarakis, "On the sensor design of torque controlled actuators: a comparison study of strain gauge and encoder-based principles," *IEEE Trans. Robot. Autom*., vol. 2, no. 2, pp. 1186-1194, Apr. 2017.
[11] Y. B. Kim, U. Kim, D.-Y. Seok, J. So, Y. H. Lee, and H. R. Choi, "Torque sensor embedded actuator module for robotic applications," *IEEE/ASME Trans. Mechatronics*, vol. 23, no. 4, pp. 1662-1672, Aug. 2018.
[12] J. W. Sensinger and R. F. Weir, "Improved torque fidelity in harmonic drive sensors through the union of two existing strategies," *IEEE/ASME Trans. Mechatronics*, vol. 11, no. 4, pp. 457-461, Aug. 2006.
[13] H. D. Taghirad, A. Helmy, and P. R. Belanger, "Intelligent built-in torque sensor for harmonic drive systems," *IEEE Instrumentation and Measurement Technology Conf. Sensing, Processing, Networking. IMTC Proc.*, vol. 2, pp. 969-974, 1997.
[14] I. Godler, "A method to compensate periodic errors by gain tuning in instrumentation," *IEEE Trans. Instrum. Meas.*, vol. 51, no. 1, pp. 37-42, Feb. 2002.
[15] B. -j. Jung, B. Kim, J. C. Koo, H. R. Choi, and H. Moon, "Joint torque sensor embedded in harmonic drive using order tracking method for robotic application," *IEEE/ASME Trans. Mechatronics*, vol. 22, no. 4, pp. 1594-1599, Aug. 2017.

[16] R. Dhaouadi, F. H. Ghorbel, and P. S. Gandhi, "A new dynamic model of hysteresis in harmonic drives," *IEEE Trans. Ind. Electron.*, vol. 50, no. 6, pp. 1165-1171, Dec. 2003.
[17] M. Ruderman and M. Iwasaki, "Sensorless torsion control of elastic-joint robots with hysteresis and friction," *IEEE Trans. Ind. Electron.*, vol. 63, no. 3, pp. 1889-1899, Mar. 2016.
[18] H. Zhang, S. Ahmad, and G. Liu, "Modeling of torsional compliance and hysteresis behaviors in harmonic drives," *IEEE/ASME Trans. Mechatronics*, vol. 20, no. 1, pp. 178-185, Feb. 2015.
[19] S. Oh and K. Kong, "High-precision robust force control of a series elastic actuator," *IEEE/ASME Trans. Mechatronics*, vol. 22, no. 1, pp. 71-80, Feb. 2017.
[20] T. T. Phuong, K. Ohishi, Y. Yokokura, and Y. Takei, "Applications of disturbance observer and Kalman filter based force sensation in motion control," in *IEEE 15th Int. Workshop on Advanced Motion Control (AMC)*, Tokyo, Japan, 2018, pp. 625-630.

**Wen-Hao, Chen** received the B.S. degree in mechanical engineering from National Sun Yat-sen University, Taiwan, in 2021, and is currently pursuing the M.S. degree in Mechanical engineering from National Taiwan University. His current research interests include robotics and mechatronics.

**Ding-Chun Hsieh** is currently pursuing the B.S. degree in Mechanical engineering from National Taiwan University. His current research interests includes robotics, vehicle dynamics.

**Jyun-Yu Lin** received the B.S. degree in mechanical engineering from National Taiwan University, Taipei. Taiwan, in 2021, and is currently pursuing the M.S. degree in Mechanical engineering from National Taiwan University. His current research interests includes robotics and mechatronics.

**Chun-Yeon Lin** received the B.S. degree in mechanical engineering from National Central University, Taoyuan, Taiwan, in 2003, the M.S. degree in electrical control engineering from National Chiao Tung University, Hsinchu, Taiwan, in 2005, the M.S. degree in mechanical engineering from Stanford University, Stanford, CA, USA, in 2011, and the Ph.D. degree in mechanical engineering from Georgia Institute of Technology, Atlanta, GA, USA, in 2017. He is currently an Assistant Professor with the Department of Mechanical Engineering, National Taiwan University, Taipei, Taiwan. His current research interests include mechatronics, sensors, robotics, and system dynamics and control.